Journal of Inorganic and General Chemistry
ZAAC
Zeitschrift für anorganische und allgemeine Chemie
doi.org/10.1002/zaac.202100209
ARTICLE

Carbothermal synthesis of micron-sized, uniform, spherical silicon carbide (SiC) particles

Tanja Feller,[a] Sabine Rosenfeldt,[b] and Markus Retsch*[a, b]

Dedicated to Prof. Dr. Josef Breu on the occasion of his 60th birthday.

Silicon carbide (SiC) particles are exciting structures because of their hardness, chemical inertness, and dielectric properties. In particular, their absorption/emission properties in the mid-infrared range render them suitable structures for ambient temperature thermal emitters. However, the synthesis of uniform, spherical structures is still challenging. Here, we present a robust synthesis procedure based on carbothermal reduction of silica precursor particles. With an isotropic shrinkage of ~30%, the spherical particle shape and uniformity are retained. Furthermore, we outline the influence of the gas atmosphere during the carbothermal treatment and demonstrate the successful conversion to SiC by electron microscopy, X-ray diffraction, thermal and optical analysis.

Introduction

Silicon carbide (SiC) is an advanced ceramic common in space but extremely rare on earth. In nature, it occurs only in negligible amounts in meteorites,[1] carborundum, or kimberlite. SiC is also termed moissanite to honor the French chemist Henri Moissan, who discovered it in 1893 during the examination of a rock from a meteor. In 1904 he identified the crystals as silicon carbide.[2] SiC shows remarkable properties like extreme hardness, high thermal conductivity, low thermal expansion, and excellent chemical inertness. The range of industrial application[3] is extensive; it ranges from the use as abrasive, for example, in sandblasting techniques or high-performance brake discs in automobiles to additives in fire-resistant materials or heating elements to modern electronic applications like semiconductors,[4] sensors,[5] field-effect transistors[6] or supercapacitors.[7] Due to the high and diverse demand, most SiC is synthetic. More than 250 polymorphs of silicon carbide are known, including various amorphous phases.[8] It has been shown that variations of size and shape can tune the optical and electrical properties of nanoscaled particles. More recently, nanostructured SiC gained attention as exciting material for passive radiative cooling. Materials with high thermal emission in the earth's 'sky window' from 8 to 13 µm and a strong reflection in the UV/Vis range can transfer thermal energy into space, thereby cooling down themselves.[9] Additionally, in dielectric particles like SiO_2, SiC, or TiO_2, surface phonon polariton (SPhP) modes can be excited.[10] This leads to absorption and emission in the desired mid-IR to far-IR range. Note that the particles' size and shape also impact the resonance of the SPhP mode and need to be controlled for optimum photonic composite structures.[11] Passive cooling effects with SiC materials have already been observed in theoretical investigations of SiO_2/SiC stacks for bandgap tuning[12] and particles in a transparent polyethylene (PE) foil[9b] as well as by a first proof of concept study[13] demonstrating the relevance of this material class for this sustainable application.

SiC particles can be fabricated by top down and bottom up methods, which address distinct particle sizes depending on the method.[14] Top-down techniques include laser ablation,[15] etching (acid, plasma, voltage),[16] and milling.[17] Ablation and etching mainly produce SiC particles in a sub 100 nm size range, whereas milling yields (sub)micron-sized beads. In case of bottom-up techniques most SiC powders are produced by a direct carbothermal reduction of silica and a carbon source, resulting in particles with a few hundred nanometers in size.[18] The general reaction is shown in equation (1):

$$SiO_2\ (s) + 3\,C \rightarrow SiC\ (s) + 2\ CO\ (g) \quad (1)$$

Thereby, the precursor silica is commonly produced by sol-gel processes,[19] which opens the possibility of adjusting particle shape, size, and morphology. Few studies have been published with silicon alkoxides as starting materials, followed by a conversion to SiC. For example, Raman et al.[20] synthesized SiC from tetraethoxysilane (TEOS), methyltriethoxysilane, or mixtures of both and with different carbon sources like phenolic resin, ethylcellulose, or starch. The obtained gels were heated to 1550 °C in an Argon atmosphere. All products from different

[a] T. Feller, Prof. Dr. M. Retsch
Department of Chemistry, Physical Chemistry I
University of Bayreuth
Universitätsstraße 30, 95447 Bayreuth, Germany
E-mail: markus.retsch @uni-bayreuth.de
[b] Dr. S. Rosenfeldt, Prof. Dr. M. Retsch
Bavarian Polymer Institute, Bayreuth Center for Colloids and Interfaces, Bavarian Center for Battery Technology
University of Bayreuth
Universitätsstraße 30, 95447 Bayreuth, Germany

Supporting information for this article is available on the WWW under https://doi.org/10.1002/zaac.202100209

precursors were found to be β-SiC with crystallite sizes from 9 to 53 nm. The density of the products was relatively low, ranging from 1.38 to 1.86 g cm^{-3}. Thorn-ball-like SiC structures from a carbonaceous silicon xerogel starting from TEOS and saccharose were prepared by Zheng et al.[21] These β-SiC particles have sizes from 100 nm to 1000 nm and a surface area up to 141 m^2 g^{-1}. Resorcinol-formaldehyde/silica composite aerogels were successfully converted to silicon carbide with average sizes of around 10 nm at reduced temperatures of ca. 700 °C by Chen et al.[22] None of these mentioned synthesis routes led to well-defined spherical morphologies. The powder-like materials consist either of polydisperse small particles with a large size distribution or are non-defined in the meso- and micron scale.

Applications based on SPhP or passive cooling require well-defined spherical particles, a shape which is in contrast to most known polymorphic structures of SiC. Narrow size distribution is paramount for fabricating functional nanophotonic structures, where the optical properties are governed by particle composition and particle distribution in a composite material. To the best of our knowledge, only three essential approaches to spherical SiC particles have been reported so far: Spherical SiC nanoparticles with average sizes from 10 to 200 nm were synthesized by fluidized bed chemical vapor deposition using hexamethyldisilane (HMDS) as a single precursor in the group of Liu et al.[23] This method was designed to achieve the continuous formation of particles in a scalable reactor environment. Hatakeyama et al.[24] and Seog et al.[25] prepared spherical silicon carbide by an acid- or base-catalyzed condensation of phenyltrimethoxysilane (PTMS) and tetraethylorthosilicate (TEOS) in water.

In this study, we managed to produce spherical SiC particles in the 700 nm to 1 μm range, which is significantly larger than most particles reported in the literature. Furthermore, the size uniformity of these refractory particles is exceptionally high, rendering them suitable for colloidal superstructures accessible by self-assembly in the future. Therefore, we combined and optimized the synthesis strategies of Hatakeyama et al.[24] and Seog et al.[25] starting with a corresponding SiO_2 precursor. We report on synthesis conditions that allow a scalable and reproducible access to such particles. Beyond potential applications in the field of catalysis, we particularly highlight the importance of SiC nanoparticles as efficient emitter materials for passive cooling applications.[26] Zhang et al.[27] found that SiC powders from silica and SiO_2–Al_2O_3 xerogels showed different polytypes depending on the reaction atmosphere. 21R SiC was synthesized under nitrogen atmosphere, whereas Argon atmosphere resulted in 12H SiC. Barbouche et al.[28] noted that air, Argon, and CO as reducing gas led to different grain sizes and variable purity of the resulting silicon carbide. Since these authors reported the reaction atmosphere as an important parameter, we additionally focused on the influence of Argon (Ar) and Nitrogen (N_2) atmosphere on the final product.

Results and Discussion

Synthesis of the SiO_2-precursor

The well-known synthesis of spherical and monodisperse silica particles was invented by Stöber[29] and refined by Bogush[30] and Giesche.[31] In these sol-gel reactions, the silica precursor TEOS is hydrolyzed in the presence of ammonia as a catalyst in a one-step process. The size distribution is controlled during synthesis by either the concentration of the reactants or the temperature and commonly results in colloidal silica with diameters from 50–2000 nm and small polydispersity. Various subsequent reports demonstrated a strong influence of TEOS concentration on the resulting particle size. When investigating small reaction batches (15 mL), we also find a strong influence of the TEOS concentration on particle size. At c = 0.125 mol L^{-1}, a bimodal distribution with a significant difference in mean particle diameter (150 nm vs. 1000 nm) was obtained. Quite notably, however, an upper limit of particle evolution exists at about $c_{TEOS} > 0.4$ mol L^{-1}, beyond which gelation occurs. Size control in this reaction is hard to achieve: for low TEOS concentrations particles with several 100 nm diameter are obtained, at intermediate TEOS concentrations small beads of a few 100 nm are accessible, and at high TEOS concentrations no particles formation is observed. Besides this, the resulting particle size is relatively insensitive to changes of the other reactants. We found that changing the concentrations of water, PTMS, and ammonia does not influence the final particle size. (Figure 1)

We attribute this behavior to the presence of PTMS, which serves as the carbon source for the subsequent pyrolysis step. PTMS influences the particle condensation kinetics. A potential reason could be the different kinetics of the alkoxy- (TEOS) and organoalkoxysilane (PTMS) condensation during the sol-gel process.[32] The phenylic group of PTMS has a higher steric hindrance and therefore affects the nucleation time (longer nucleation time) and the formation of a three-dimensional silica network. The chemical structure of TEOS exhibits four equivalent side chains and is, therefore, expected to induce more nucleation sites (corresponding to a shorter nucleation time) compared to the former one. PTMS can also act as a surfactant in this process, due to its hydrophilic silanol headgroup and its permanently attached hydrophobic phenyl group, which may affect the particle size and its porosity.

Changing the ammonia concentration in the synthesis from 0.25 mol L^{-1} up to 2.0 mol L^{-1} at a constant PTMS and TEOS concentration (at 0.25 mol L^{-1} and 0.0625 mol L^{-1}, respectively) did not influence the diameter of the particles. It resulted in diameters of about 750 nm for all particles (Figure 1b). In literature opposing statements on the influence of ammonia can be found.[24–25]

Also, the concentration of PTMS only marginally influences the resulting particle size (Figure 1c). Beyond a concentration of 0.2 mol L^{-1}, all samples range around 800 nm.

Changing the volume ratio of PTMS:H_2O as proposed by Segers et al.[33] to increase the particle diameter with a higher amount of water had no significant impact on the size but

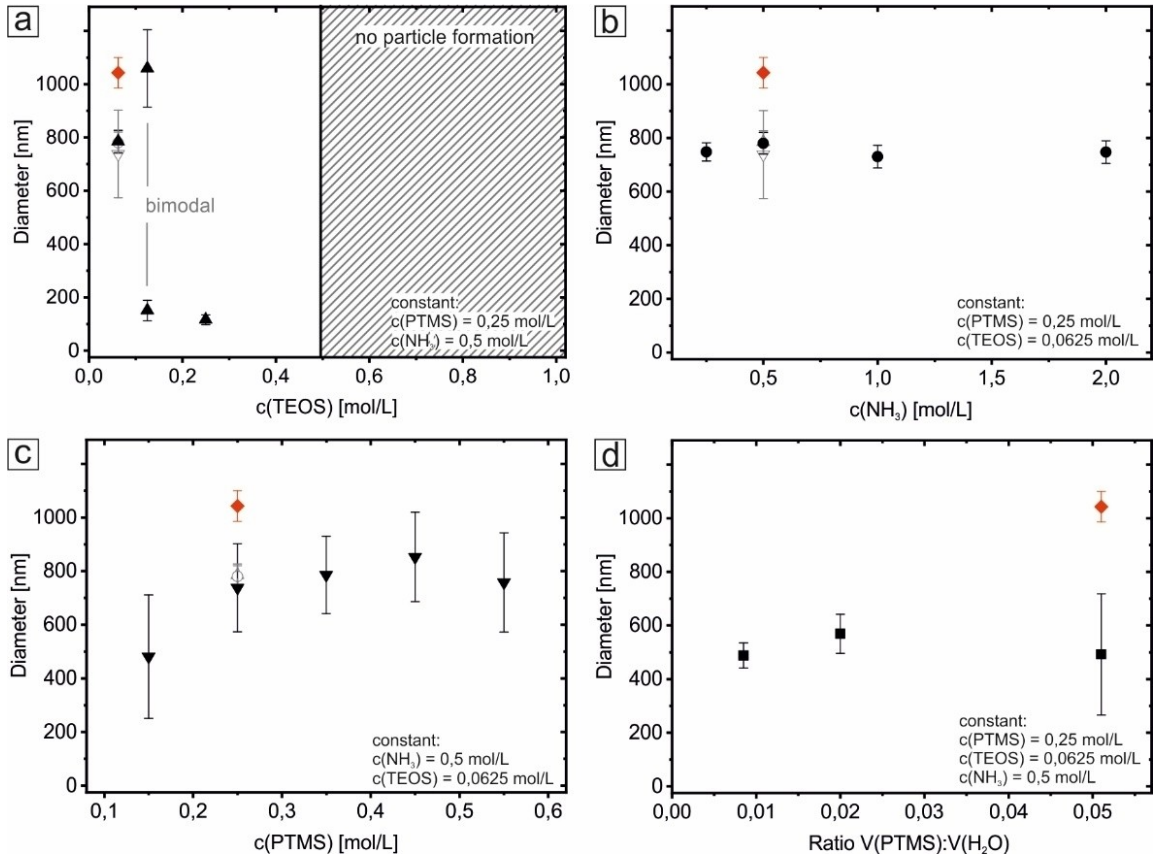

Figure 1. Diameter variations of the particle dependent on the concentration of TEOS (a), ammonia (b), PTMS (c), and the volume ratio of PTMS and H_2O (d). The data points marked in red used a total volume of 150mL; all other syntheses (black symbols) were conducted in small batches with mostly 15 mL. Error bars indicate the standard deviation of the particles.

instead on the size distribution (Figure 1d). The deviation of the particle diameter increased by around 35% from low to high water content.

We deduced optimum reactant concentrations from these screening reactions, which are $c_{TEOS} = 0.0625\ mol\,L^{-1}$, $c_{PTMS} = 0.25\ mol\,L^{-1}$ and $c_{NH3} = 0.5\ mol\,L^{-1}$. In combination with a ten-fold upscaling of the reaction volume, we synthesized SiC-precursor particles with a size of 1043 ± 57 nm and narrow size distribution. The deviation from the small-batch screening syntheses is caused by subtle changes to the nucleation kinetics owing to the larger reaction vessel. We will outline the carbothermal reduction process and properties of these scaled-up precursor particles in the following paragraphs.

Carbothermal reduction to SiC

The carbothermal heat treatment is the second step to obtain SiC particles. The crucial point is not only to successfully convert the precursor to silicon carbide but also to retain the spherical shape of the particles. Further, stoichiometry, the porosity of the carbon component[34] and the silica/carbon interface play a significant role in the process since enough carbon must be near the silicon atoms to hinder the formation of other derivates like pure silicon. Such side reactions were, for example, mentioned by Filsinger et al.,[18] and Biernacki et al.,[35] who investigated the formation of SiC and side reactions in general. An excess of C relative to Si is introduced by the phenyl ring of PTMS (see supporting information). We note that control experiments (not shown here) with grained mixtures of pure submicron sized SiO_2 particles and graphite powder did not result in SiC particles. This underlines the importance of an intimate mixture of silica and carbon, which has been obtained from a bottom-up approach in our case and led to covalent bonding between the Si and C source by the condensation reaction.

Along the same line, Shcherban et al.[36] showed the formation of porous SiC using grained mixtures of mesoporous silica (particle size < 100 nm) and sucrose as carbon source. While the resulting composite in this case can still be considered a grained mixture, the surface area is high owing to the sub 100 nm particle size. The intimate contact between silica and carbon in this case allowed the authors a successful conversion to SiC.

To convert the SiO_2 precursor into SiC, we heated the powder samples to 1500 °C (heating rate 20 K min^{-1}) for 4 h in an Ar or N_2 atmosphere (flow rate 50 mL min^{-1}, 1 bar). Subsequently, the SiC was purified from excess carbon species

by post-thermal treatment (air, 800 °C, 4 h) and characterized with SEM (Figure 2).

The SiO_2-precursor (SiO_2-Ph) consists of spherical particles with smooth surface and a mean diameter of $D = 1043 \pm 57$ nm, $\sigma = 5.4\%$ (standard deviation of a Gaussian size distribution). The resulting particles in Ar and N_2 have a diameter of 710 ± 38 nm ($\sigma = 5.3\%$) and 769 ± 41 nm ($\sigma = 5.3\%$), respectively. After the carbothermal reduction, the spherical shape is well preserved. This contrasts with other studies,[37] where it is pointed out that carbothermal reduction is a non-pseudomorphic transformation process. We noticed a considerable shrinkage of about 30% in particle size.

The shrinkage behavior of metal oxide precursors is already known; for example, Chen et al.[22] noticed shrinkage of 21% after thermal conversion of C/SiO_2 to SiC aerogels and Lechner et al.[38] determined a reduction of up to 18% by calcination of TiO_2 to anatase. The size reduction is related to the release of gaseous species during the transformation process, particularly H_2O and CO, leading to a higher density and a considerable mass loss. Biernacki et al.[35] reported a two-step reaction pathway with gaseous CO and SiO as intermediates during the formation of SiC from SiO_2. For the possible intermediate Silicon (Si),[39] a shrinkage of the crystal lattice due to the formation of vacancies is known.[27] The variety of potential intermediates[40] also opens the possibility of side reactions and deviations from the targeted SiC composition. In this context, reactions with the atmosphere are possible; for example, at high temperatures from 1400–1450 °C, silicon dioxide can be converted to Si_3N_4 by a carbothermal reduction in N_2 atmosphere.[41]

$$3\ SiO_2\ (s) + 6\,C + 2\,N_2 \rightarrow Si_3N_4\ (s) + 6\ CO\ (g) \quad (2)$$

The particles (Figure 2b and c) exhibit different surface morphologies: rough (b, in Ar) and smooth (c, in N_2), demonstrating a significant influence of the atmosphere during the thermal treatment. Particles synthesized in an Ar environment seem to be coarsely grained, leading to a granular microstructure. The individual grains have approximately a size of 50 nm. We interpret these grains as crystallites of SiC. In contrast, the surfaces of the particles shown in Figure 2c are very smooth. No grain-like structures are detected, which we attribute to the rather amorphous microstructure even after pyrolysis. In rare cases, round areas (arrow in Figure 2c) or residuals from neighboring microparticles (Figure S3) are visible. Such artifacts originate from the sinter processes among adjacent particles. N_2 adsorption isotherms (Figure S5) of the precursor and pyrolyzed particles reveal strongly different BET surface areas and hystereses. Whereas the precursor, SiC commercial, and SiC Ar pyrolyzed can be regarded as non-porous materials, the pyrolysis under N_2 conditions results in an appreciable surface area of ~270 $m^2 g^{-1}$. This large surface area is likely to be caused by the conical pores between clustered particles and by PTMS-templated pores in the mesoporous range.

To get a more profound insight into the atmospheric impact on the carbothermal process, simultaneous thermal analysis (STA) measurements were performed in Ar and N_2 at 1300 °C, 1400 °C, and 1500 °C (Figure 3). The general trend is similar in all samples, in detail: (a) The mass loss comprises two main steps. The first occurs right at the beginning of the heating ramp and reveals a mass loss of about 25%. The second mass loss begins after 50 min at ca. 1000 °C. According to Seog et al.[25] the first step results from the loss of crystal water of SiO_2 and the second from the decomposition of the precursor phenyl groups.

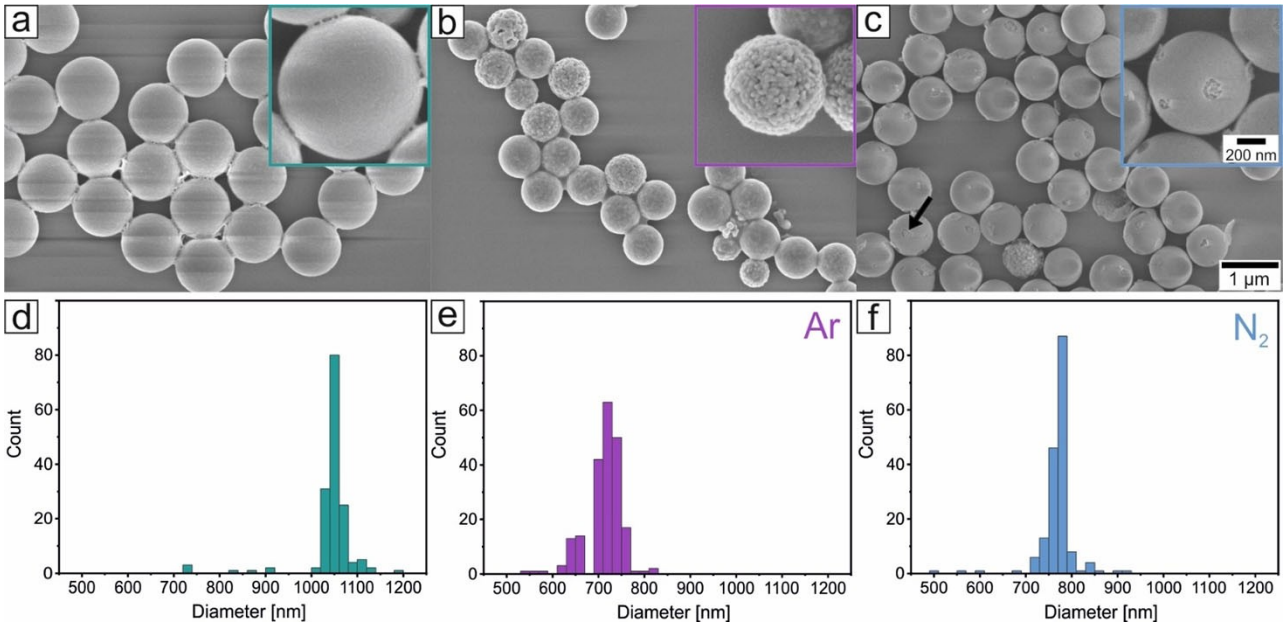

Figure 2. SEM images of the precursor particles (a), the particles reacted in Ar (b), and N_2 (c) with a magnified image of one particle as inset. The corresponding size distributions (d-f) are below.

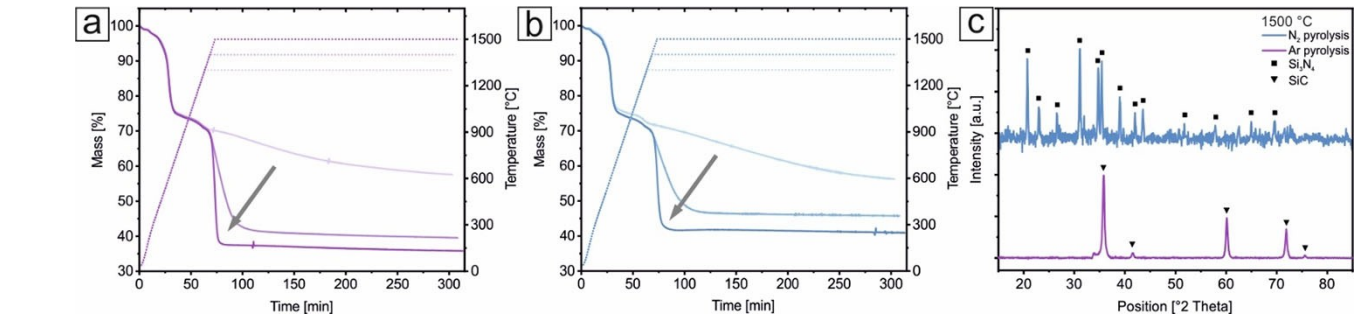

Figure 3. STA measurements of the carbothermal reduction of SiO_2-PTMS precursor particles in Ar (a) and N_2 (b) atmosphere at three different temperatures (bright to dark). Results of XRD measurements (c) of the Ar and N_2 pyrolysis samples at 1500 °C.

(b) It can be noticed that with increasing temperature, the second mass loss step is happening more abruptly. This second mass loss strongly depends on the pyrolysis temperature and requires >1400 °C. The total mass loss depends on the atmosphere of the pyrolysis environment, with the Ar atmosphere leading to higher losses as compared to N_2. For 1500 °C, 1400 °C, and 1300 °C in Ar, we find a residual mass of 35.8 %, 39.6 %, and 57.6 %, respectively. In N_2, we found 40.9 %, 45.8 %, and 56.3 % of the residual mass, respectively.

The decrease in residual mass with increasing temperature suggests a more complete reaction at 1500 °C.

A possible explanation for the lower values of the residual mass in the case of Ar atmosphere could be that (a) the conversion of SiO_2 to SiC in N_2 has a slower kinetic or (b) that a more complex reaction pathway inhibits the conversion in N_2 with the formation of side-products.

These assumptions were underlined by X-ray diffraction (XRD) data (Figure S1). With increasing temperature, more and better-defined Bragg peaks are visible. Chu et al. saw a similar influence on the reaction temperature.[42] Compared to industrial SiC powder, the crystallites are significantly smaller, which can be inferred by the broader peak width of the Bragg peaks. The XRD pattern of the industrially produced powder can be described by a mixture of hexagonal (71 %[43]) and cubic (29 %[44]) SiC. An SEM image of this powder is given in Figure S2, demonstrating the non-spherical morphology of this sample.

The XRD data of samples prepared at 1300 °C (Figure S1a–b) shows no Bragg peaks, but a high monotonically increasing intensity for $2\theta > 10°$, and a broad shoulder at 2θ around 22°. The shoulder at ~22° is also present in the amorphous SiO_2-Ph precursor (Figure S1d). Note that the peak seen in the pattern of SiO_2-Ph at $2\theta \approx 7°$ is missing, indicating the structural transformation of the precursor. This is in good accordance with the results of the STA, where the first mass loss occurred already around 570 °C. The peak positions of the sample prepared at 1500 °C in Ar are consistent with the expected positions of SiC,[45] whereas the sample prepared at 1500 °C in N_2 hints at a mixture of SiC[46] and Si_3N_4.[47] The particles in Ar display five prominent peaks at $2\theta = 35.8$, 41.5, 60.2, 71.9, and 75.7°, which can be identified as SiC. Stacking faults can explain the low-intensity peak at $2\theta = 33.2°$.[48]

It is known that a huge number of SiC polymorphs exist and that during the transformation, intermediates of multiple different Si-species (SiC, SiO_2, SiO, Si) and side reactions can occur.[40] A precise assignment of the polytypes and their respective ratios in the obtained submicron sized particles is impossible based on this XRD analysis. Nevertheless, the significant influence of the gaseous atmosphere on the structure of the particles is confirmed.

The formation of a sizeable amount of Si_3N_4 in the case of a carbothermal reaction in N_2 atmosphere is confirmed by scanning electron microscopy-electron diffraction spectroscopy (SEM-EDS) measurements (1500 °C, Ar or N_2, and precursor, Figure S4). We find carbon, silicon, and oxygen species as the main compounds for the precursor and the samples transformed in Ar. Additionally, in an N_2 atmosphere, a significant amount of N is present. In all cases, the elemental distribution is homogeneously spread across the particles, and no areas of distinct crystallites, enriched or depleted areas, can be discerned (Figure S4). A quantitative assessment of the elemental composition is hardly possible, in particular, since a carbon-coated grid had to be used for immobilizing the particles. However, we can qualitatively conclude that under Ar atmosphere conditions, submicron sized SiC particles of retained spherical shape could be accessed. In contrast, an N_2 atmosphere results in an incomplete transformation with a particular portion of Si_3N_4 as a side product. The successful conversion to SiC is additionally confirmed by the particle properties, which are outlined below.

The densities were investigated in a Helium pycnometer and are given in Table 1. In literature SiC has a density of about $\rho = 3.21$ g cm^{-3}.[49] Silicon nitride has a density of 3.17 g cm^{-3}[50]

Table 1. Thermal properties and density of the particles.

	Effusivity [W s$^{1/2}$ m^{-2} K^{-1}]	Thermal conductivity [W m^{-1} K^{-1}]	Density [g cm^{-3}]
SiO_2-PTMS precursor	152.07	0.066	1.294 ± 0.003
SiC-Ar pyrolysis	136.56	0.063	2.894 ± 0.019
SiC-N_2 pyrolysis	102.62	0.055	2.258 ± 0.027
SiC-commercial	175.66	0.072	2.923 ± 0.013

and amorphous silica of $\rho = 2.12 g cm^{-3}$.[50] We measured densities of $\rho = 1.3\ g\,cm^{-3}$, 2.3. g cm^{-3}, $2.9\ g\,cm^{-3}$, and $2.9\ g\,cm^{-3}$ for the precursor (starting material), the samples in N_2 and Ar, and the industrial powder. Note that both pure SiC samples have comparable densities. The fact that the material obtained in N_2 has a lower density than pure SiC is consistent with the observation of a mixture of unreacted precursor, SiC, and Si_3N_4 (cf. results of XRD and STA).

Next, we examined the thermal properties of all samples. The specific heat (c_p) (Figure 4) is determined according to ASTM E 1269 and shows a continuous increase from around −30 °C to 250 °C. At ambient temperature, our synthesized SiC particles in Ar have $0.427\ J\,g^{-1}\,C^{-1}$, almost the same specific heat value as the industry SiC powder ($c_p = 0.446\ J\,g^{-1}\,C^{-1}$). In literature[49] for hexagonal SiC a value of $c_p = 0.69\ J\,g^{-1}\ C^{-1}$ is reported. A possible reason for the discrepancy of these values could be the different SiC polymorphs in combination with different shapes and particle sizes. The silica precursor particles with phenyl groups have a distinctly higher heat capacity with

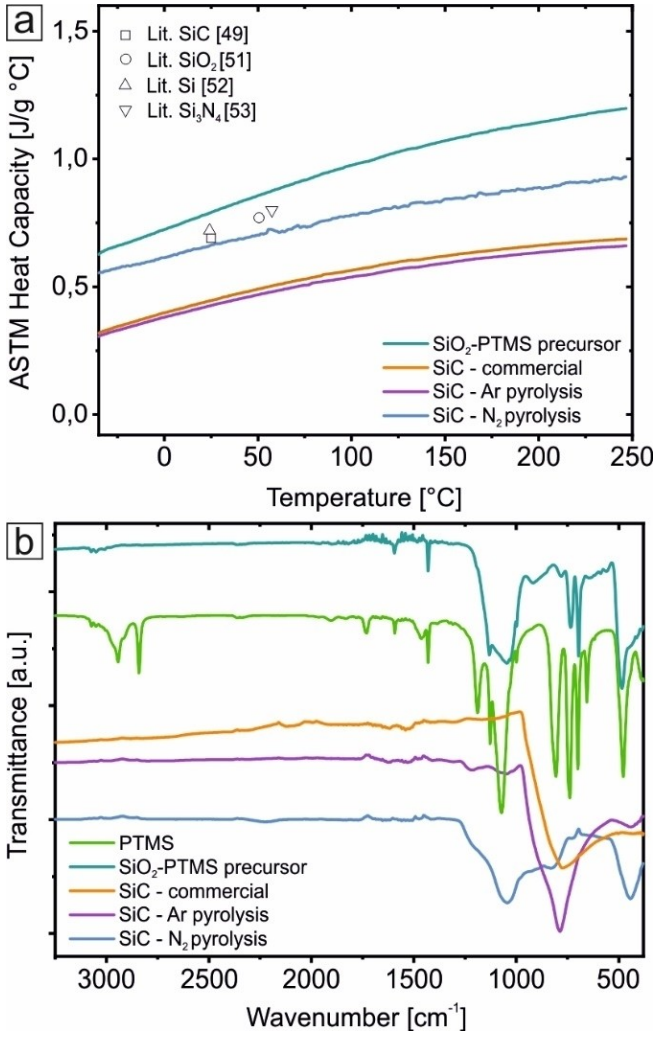

Figure 4. Comparison of the specific heat data (a) and the transmission IR spectra plotted as offset (b) of the industry SiC powder, PTMS, precursor particles, particles fabricated in Ar, and in N_2.

$0.790\ J\,g^{-1}\,C^{-1}$, comparable to silica literature values.[51] Furthermore, the sample synthesized in N_2 lies with $0.663\ J\,g^{-1}\,°C^{-1}$ in between and can be assigned to silicon nitride[52] or silicon.[53]

The powders' effusivity and thermal conductivity were investigated with a modified transient plane source method (MTPS)[54] with a constant compressive force of 5 N. Here, the industry SiC powder has the highest value, followed by the precursor particles and the Ar sample, and finally, the N_2 sample with the lowest values (Table 1). The thermal conductivity at 300 K for bulk 3 C-SiC in literature[49] is $k = 3.6\ W\,cm^{-1}\,C^{-1}$, which is about a factor of 50 higher than the values obtained for this microstructured powder. In powders, such low values are often obtained and are a consequence of the constriction resistance at the interparticle contact area.[55] Considering the chemical variability of the samples, the obtained differences in effusivity and thermal conductivity for the industrial SiC, SiC in Ar, and for the precursor are negligible and in the same range. Differences among the samples have to be attributed to subtle differences in the interparticle contact area rather than the corresponding bulk material behavior.

We investigated the optical properties and, in particular, the suitability of these powders as efficient thermal emitters by Fourier transformation infra-red (FT-IR) spectroscopy (Figure 4). The SiO_2-Ph precursor shows characteristic bands of both silica and pure PTMS. For example, the –C–O–H vibration at 1130 cm^{-1} and the phenyl ring deformation vibrations from 736 cm^{-1} to 698 cm^{-1} and 482 cm^{-1}.[56] In accordance with density, c_p, and XRD data, the precursor is confirmed as at least a mixture of the two constituents after their condensation reaction, TEOS and PTMS. The industrial SiC and SiC-rich samples (Ar, 1500 °C) exhibit a strong absorption band at $\nu =$ 785 cm^{-1}, which is characteristic of the Si–C stretching mode.[57] The uniform spherical particles exhibit a more distinct peak at the Si–C stretching mode, which renders them particularly suitable for fabricating a selective emitter in this spectral range.[26] All other samples (N_2, precursor, and PTMS) show an absorption band at 1037 cm^{-1}, assigned to asymmetric Si–O vibration.[58] Additionally, the sample prepared in N_2 has small bands at $\nu = 831\ cm^{-1}$ and 441 cm^{-1}. According to literature, amorphous Si_3N_4 has a broad absorption band at around 840 cm^{-1}.[59] The 441 cm^{-1} band can also be assigned to β-Si_3N_4.[60] These findings align with the previous measurements and corroborate that the sample prepared in N_2 is a mixture of the unreacted silica precursor and silicon nitride.

The complementary absorption properties of the Si_3N_4 compared to the SiC particles, may turn out to be particularly useful for passive cooling applications. As outlined above simple mixtures of these two particle powders would allow to design various emission properties in the sky window range and thereby access materials that can perform as selective or broadband emitting material.

Conclusions

We demonstrated the successful synthesis of spherical SiC particles in a size range from 700 nm to 1 μm. The key

component in this carbothermal reduction process is the usage of PTMS during the sol-gel fabrication of the precursor particles. The presence of PTMS influences the nucleation and growth kinetics of the particle formation step such that uniform precursor beads are obtained in a size range from 700 nm to 1 μm with a notable robustness to variations of the reactant concentrations. The carbothermal reduction proceeds in an isomorphic manner and results in uniformly shrunk (~30%) microparticles. Ar as the inert atmosphere is paramount to drive the SiC conversion to completion, which we characterized by XRD, pycnometry, DSC, and IR spectroscopy. A N_2 environment during carbothermal reduction, in contrast, inhibits the SiC formation and leads to a mixture of SiO_2 and Si_3N_4 as side reactions. The established protocol to well-defined SiC beads is of high relevance to build nanophotonic structures with controllable properties in the mid-infrared range.

Experimental Section

Materials

Tetraethylorthosilicate (TEOS, Sigma-Aldrich GmbH, for synthesis), Trimethoxyphenylsilane (PTMS, Sigma-Aldrich GmbH, 97%), Ammonia (NH_3, Honeywell Chemicals, 30–33% solution in water), and silicon carbide powder (ESK-SIC GmbH) were used as received. Millipore water was taken from a Millipore Direct Q3UV unit (Merck Millipore).

Particle synthesis

Ammonia was mixed with water and stirred at room temperature for 20 min to equilibrate the solution. Then, the desired amount of PTMS and TEOS were added quickly, one after the other (Table 2). The reaction was stirred at 550 rpm for 10 minutes. Afterwards, the stirring was shut off, and the mixture was allowed to ripen overnight. All used concentrations and volumes for the experiments are shown in Table 2. The resulting particles were washed two times with H_2O and then dried on a heating plate.

Table 2. Concentrations and volumes of the educts in the performed syntheses.

Experiment	V_{total} [mL]	$c(NH_3)$ [mol L^{-1}]	c(TEOS) [mol L^{-1}]	c(PTMS) [mol L^{-1}]	$c(H_2O)$ [mol L^{-1}]
A	15	0.25	0.0625	0.25	55.5
B	15	0.5	0.0625	0.25	55.5
C	15	1.0	0.0625	0.25	55.5
D	15	2.0	0.0625	0.25	55.5
E	15	0.5	0.125	0.25	55.5
F	15	0.5	0.25	0.25	55.5
G	15	0.5	0.5	0.25	55.5
H	15	0.5	1.0	0.25	55.5
I	15	0.5	0.0625	0.15	55.5
J	15	0.5	0.0625	0.25	55.5
K	15	0.5	0.0625	0.35	55.5
L	15	0.5	0.0625	0.45	55.5
M	15	0.5	0.0625	0.55	55.5
N	14.55	0.5	0.0625	0.25	55.5
O	38.5	0.5	0.0625	0.25	55.5
P	90.8	0.5	0.0625	0.25	55.5
Q	150	0.5	0.0625	0.25	55.5

For the carbothermal reduction, the particles were placed in an alumina boat in a tube furnace. They were heated to 1500 °C with 20 K min^{-1} in a N_2 or Ar atmosphere with a continuous gas flow of 50 mL min^{-1}. After cooling down, the particles were heated again to 800 °C for 4 h in air to burn most of the excess carbon away.

Methods

Simultaneous thermal analysis: A Netzsch model STA 449 F3 coupled with a Bruker Alpha II FT-IR spectrometer was used for thermal characterization. The measurements were performed in Al_2O_3 crucibles to 1300 °C, 1400 °C, and 1500 °C with a heating rate of 20 K min^{-1} in N_2 and Ar atmosphere.

Thermal treatment reactions were performed in an alumina boat inside a Nabertherm RHTC-50-150/17 tube furnace with a heating rate of 20 K min^{-1} in N_2 and Ar atmosphere at 1500 °C.

Scanning electron microscopy: Images were taken with a Zeiss Ultra plus (Carl Zeiss AG, Germany) at an operating voltage of 3 kV and with in-lens detection after sputtering with 2 nm of platinum. For EDS analysis, the particles were prepared onto TEM Cu grids (Plano GmbH) with a carbon film and investigated with an operating voltage of 10 kV with a STEM sample holder to reduce the background. A Thermo Scientific™ UltraDry™ EDS X-ray detector was used.

The diameter of the particles was evaluated using a MATLAB circle detection function of at least 150 particles. The search parameters were optimized manually.

Density analysis was carried out with a Quantachrome Ultrapyc 1200e in Helium gas.

Differential scanning calorimetry measurements were performed with a DSC 2500 from TA Instruments, and the specific heat was calculated according to ASTM E 1269.

X-ray powder diffraction patterns were recorded in Bragg-Brentano geometry on an Empyrean diffractometer (PANalytical B.V.; Netherlands) using Cu–K_α radiation ($\lambda = 1.54187$ Å). If needed, the data were corrected for amorphous background and indexed with the software provided on the instrument.

Thermal conductivity and effusivity were determined with the C-Term TCi Thermal Conductivity Analyzer. Samples were tested with 5 N compression.

Fourier transform infrared spectroscopy (FT-IR) was conducted on the dried samples in attenuated total reflectance (ATR) mode on a Bruker Vertex70 Spectrometer from 7500 cm^{-1} to 380 cm^{-1}. For each spectrum, 64 scans were averaged, and a spectral resolution of 4 cm^{-1} was used.

Nitrogen sorption measurements were carried out on a Quantachrome Autosorb AS-1 pore analyzer at 77 K. Prior to the measurements, all samples were preconditioned in a vacuum at 120 °C for 12 hours. For the analysis, the Quantachrome ASiQ v3.0 software was used. The specific surface areas were calculated using the BET method.

Funding

This project has received funding from the European Research Council (ERC) under the European Union's Horizon 2020

research and innovation program (grant agreement no. 714968).

Acknowledgments

We thank Stefan Rettinger for the help with STA and DSC experiments, Patrick Länger and Prof. Dr. Jürgen Senker for the BET measurements and the Bavarian Polymer Institute, especially Martina Heider and Dr. Ulrich Mansfeld, for helping with SEM-EDS measurements. Open Access funding enabled and organized by Projekt DEAL.

Conflict of Interest

The authors declare no conflict of interest.

Keywords: thermal emitter · refractory material · isomorphic conversion · surface phonon polariton · mid-infrared emission

[1] J. Bauer, J. Fiala, R. Hřichová, *Am. Mineral.* **1963**, *48*, 620–634.
[2] H. Moissan, *C. R. Acad. Sci.* **1905**, *140*, 405–406.
[3] S. E. Saddow, A. Agarwal, *Advances in silicon carbide processing and applications*, Artech House, Boston, **2004**.
[4] R. Gerhardt, *Properties and Applications of Silicon Carbide*, InTech, Rijeka, **2011**.
[5] N. G. Wright, A. B. Horsfall, K. Vassilevski, *Mater. Today* **2008**, *11*, 16–21.
[6] H.-K. Seong, H.-J. Choi, S.-K. Lee, J.-I. Lee, D.-J. Choi, *Appl. Phys. Lett.* **2004**, *85*, 1256–1258.
[7] L. Gu, Y. Wang, Y. Fang, R. Lu, J. Sha, *J. Power Sources* **2013**, *243*, 648–653.
[8] R. Cheung, *Silicon Carbide Microelectromechanical Systems for Harsh Environments*, Imperial College Press, London, **2006**.
[9] a) A. P. Raman, M. A. Anoma, L. Zhu, E. Rephaeli, S. Fan, *Nature* **2014**, *515*, 540–544; b) A. R. Gentle, G. B. Smith, *Nano Lett.* **2010**, *10*, 373–379.
[10] J. D. Caldwell, L. Lindsay, V. Giannini, I. Vurgaftman, T. L. Reinecke, S. A. Maier, O. J. Glembocki, *Nat. Photonics* **2015**, *4*, 44–68.
[11] S. K. Andersson, G. A. Niklasson, *J. Phys. Condens. Matter* **1995**, *7*, 7173–7184.
[12] E. Rephaeli, A. Raman, S. Fan, *Nano Lett.* **2013**, *13*, 1457–1461.
[13] A. S. Alketbi, B. Yang, A. Raza, M. Zhang, J.-Y. Lu, Z. Wang, T. Zhang, *J. Photonics Energy* **2018**, *9*.
[14] M. O. de Vries, S. i. Sato, T. Ohshima, B. C. Gibson, J. M. Bluet, S. Castelletto, B. C. Johnson, P. Reineck, *Adv. Opt. Mater.* **2021**.
[15] a) S. Yang, B. Kiraly, W. Y. Wang, S. Shang, B. Cao, H. Zeng, Y. Zhao, W. Li, Z. K. Liu, W. Cai, T. J. Huang, *Adv. Mater.* **2012**, *24*, 5598–5603; b) J. Zhu, S. Hu, W.-w. Xia, T.-h. Li, L. Fan, H.-t. Chen, *Mater. Lett.* **2014**, *132*, 210–213.
[16] a) H. Lin, J. A. Gerbec, M. Sushchikh, E. W. McFarland, *Nanotechnology* **2008**, *19*, 325601; b) Y. Zakharko, T. Serdiuk, T. Nychyporuk, A. Géloën, M. Lemiti, V. Lysenko, *Plasmonics* **2012**, *7*, 725–732; c) X. L. Wu, J. Y. Fan, T. Qiu, X. Yang, G. G. Siu, P. K. Chu, *Phys. Rev. Lett.* **2005**, *94*, 026102.
[17] B. M. Madhusudan, H. P. Raju, S. Ghanaraja, G. N. Sudhakar, *J. Inst. Eng. India Ser. D* **2021**, *102*, 167–172.
[18] D. H. Filsinger, D. B. Bourrie, *J. Am. Ceram. Soc.* **1990**, *73*, 1726–1732.
[19] C. J. Brinker, G. W. Scherer, *Sol-gel science : the physics and chemistry of sol-gel processing*, Academic Press, Boston, **1990**.
[20] V. Raman, O. P. Bahl, U. Dhawan, *J. Mater. Sci.* **1995**, *30*, 2686–2693.
[21] Y. Zheng, Y. Zheng, L.-X. Lin, J. Ni, K.-M. Wei, *Scripta Mater.* **2006**, *55*, 883–886.
[22] K. Chen, Z. Bao, A. Du, X. Zhu, G. Wu, J. Shen, B. Zhou, *Microporous Mesoporous Mater.* **2012**, *149*, 16–24.
[23] R. Z. Liu, M. L. Liu, J. X. Chang, *J. Nanopart. Res.* **2017**, *19*.
[24] F. Hatakeyama, S. Kanzaki, *J. Am. Ceram. Soc.* **1990**, *73*, 2107–2110.
[25] I. S. Seog, C. H. Kim, *J. Mater. Sci.* **1993**, *28*, 3277–3282.
[26] X. Yu, J. Chan, C. Chen, *Nano Energy* **2021**, *88*.
[27] B. Zhang, J. Li, J. Sun, S. Zhang, H. Zhai, Z. Du, *J. Eur. Ceram. Soc.* **2002**, *22*, 93–99.
[28] M. Barbouche, R. Benabderrahmane Zaghouani, N. E. Benammar, K. Khirouni, H. Ezzaouia, *Int. J. Adv. Manuf. Technol.* **2016**, *91*, 1339–1345.
[29] W. Stöber, A. Fink, E. Bohn, *J. Colloid Interface Sci.* **1968**, *26*, 62–69.
[30] G. H. Bogush, M. A. Tracy, C. F. Zukoski, *J. Non-Cryst. Solids* **1988**, *104*, 95–106.
[31] H. Giesche, *J. Eur. Ceram. Soc.* **1994**, *14*, 189–204.
[32] a) T. Jermouni, M. Smaihi, N. Hovnanian, *J. Mater. Chem.* **1995**, *5*, 1203–1208; b) C. Wu, Y. Wu, T. Xu, W. Yang, *J. Non-Cryst. Solids* **2006**, *352*, 5642–5651.
[33] M. Segers, N. Arfsten, P. Buskens, M. Möller, *RSC Adv.* **2014**, *4*, 20673–20676.
[34] N. Shcherban, S. Filonenko, S. Sergiienko, P. Yaremov, M. Skoryk, V. Ilyin, D. Murzin, *Int. J. Appl. Ceram. Technol.* **2018**, *15*, 36–41.
[35] J. J. Biernacki, G. P. Wotzak, *J. Am. Ceram. Soc.* **1989**, *72*, 122–129.
[36] N. D. Shcherban, S. M. Filonenko, P. S. Yaremov, S. A. Sergiienko, V. G. Ilyin, D. Y. Murzin, *J. Mater. Sci.* **2016**, *52*, 3917–3926.
[37] J. Su, B. Gao, Z. Chen, J. Fu, W. An, X. Peng, X. Zhang, L. Wang, K. Huo, P. K. Chu, *ACS Sustainable Chem. Eng.* **2016**, *4*, 6600–6607.
[38] A. M. Lechner, T. Feller, Q. Song, B. A. F. Kopera, L. Heindl, M. Drechsler, S. Rosenfeldt, M. Retsch, *Colloid Polym. Sci.* **2020**, *298*, 867–878.
[39] V. D. Krstic, *J. Am. Ceram. Soc.* **1992**, *75*, 170–174.
[40] B. Abolpour, R. Shamsoddini, *Prog. React. Kinet. Mec.* **2019**, *45*, 1–14.
[41] F. L. Riley, *J. Am. Ceram. Soc.* **2004**, *83*, 245–265.
[42] A. Chu, M. Qin, D. Li, H. Wu, Z. Cao, X. Qu, *Mater. Chem. Phys.* **2014**, *144*, 560–567.
[43] N. W. Thibault, *Am. Mineral.* **1944**, *29*, 327–362.
[44] H. Brækken, *Z. Kristallogr. Cryst. Mater.* **1932**, *81*, 309–313.
[45] A. L. Hannam, P. T. B. Shaffer, *J. Appl. Crystallogr.* **1969**, *2*, 45–48.
[46] P. Krishna, A. R. Verma, *Acta Crystallogr.* **1962**, *15*, 383–387.
[47] D. A. Norris, M. A. Rodriguez, S. K. Fukuda, R. L. Snyder, *Powder Diffr.* **1990**, *5*, 225–226.
[48] K. Koumoto, S. Takeda, C. H. Pai, T. Sato, H. Yanagida, *J. Am. Ceram. Soc.* **1989**, *72*, 1985–1987.
[49] M. E. Levinshtein, S. L. Rumyantsev, M. Shur, *Properties of advanced semiconductor materials: GaN, AlN, InN, BN, SiC, SiGe*, Wiley, New York, **2001**.
[50] W. M. Haynes, D. R. Lide, *CRC Handbook of Chemistry and Physics*, 92nd ed., CRC Press, Boca Raton, Fl., **2011**.
[51] H. Moser, *Phys. Z.* **1937**, *37*, 737–753.
[52] K.-P. Jen, R. Warzoha, J. Guo, M. Tang, S. Santhanam, *J. Nanomater.* **2013**, *2013*, 7.
[53] J. P. Dismukes, L. Ekstrom, E. F. Steigmeier, I. Kudman, D. S. Beers, *J. Appl. Phys.* **1964**, *35*, 2899–2907.

[54] N. Mathis, *High Temp. High Press.* **2000**, *32*, 321–327.
[55] D. J. Cumberland, R. J. Crawford, *The packing of particles*, Elsevier, Amsterdam, **1987**.
[56] G. Socrates, *Infrared and Raman Characteristic Group Frequencies: Tables and Charts*, 3rd ed., Wiley, **2004**.
[57] N. G. Dhere, J. H. Wohlgemuth, R. Jones-Albertus, A. Kleinová, J. Huran, V. Sasinková, M. Perný, V. Šály, J. Packa, in *Reliability of Photovoltaic Cells, Modules, Components, and Systems VIII*, **2015**.
[58] P. Innocenzi, *J. Non-Cryst. Solids* **2003**, *316*, 309–319.
[59] P. J. Launer, B. Arkles, in *Silicon Compounds: Silanes and Silicones*, Gelest Inc., Morrisville, PA, USA, **2013**, pp. 175–178.
[60] V. N. Antsiferov, V. G. Gilev, V. I. Karmanov, *Refract. Ind. Ceram.* **2003**, *44*, 108–114.

Manuscript received: June 16, 2021
Revised manuscript received: September 8, 2021
Accepted manuscript online: September 9, 2021

ARTICLE

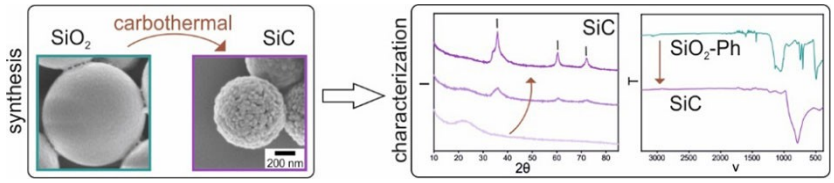

*T. Feller, Dr. S. Rosenfeldt, Prof. Dr. M. Retsch**